First-principles investigation of two-dimensional trichalcogenide and sesquichalcogenide monolayers

L. Debbichi,[1,*] H. Kim,[1] T. Björkman,[2] O. Eriksson,[3] and S. Lebègue[4,†]

[1]*Graduate School of Energy, Environment, Water, and Sustainability (EEWS), Korea Advanced Institute of Science and Technology (KAIST), Yuseong-gu, Daejeon 305-701, Korea*

[2]*Physics/Department of Natural Sciences, Åbo Akademi University, Porthansgatan 3, 20500 Turku, Finland*

[3]*Department of Physics and Astronomy, Box 516, Uppsala University, SE-751 20 Uppsala, Sweden*

[4]*Laboratoire de Cristallographie, Résonance Magnétique et Modélisations (CRM2, UMR CNRS 7036) Institut Jean Barriol, Université de Lorraine BP 239, Boulevard des Aiguillettes, 54506 Vandoeuvre-lès-Nancy, France*

(Received 28 February 2016; revised manuscript received 27 May 2016; published 24 June 2016)

We have used density functional theory to investigate the dynamical stability and the electronic structure of several new semiconducting two-dimensional single layers, with chemical compositions such as ABX_3 and A_2X_3. The calculated interlayer binding energies and the absence of imaginary states in the phonon spectra indicate the possibility to isolate them in the form of a single layer. Also, the calculated band edges reveal that some of these two-dimensional materials are promising candidates for water-splitting applications.

DOI: 10.1103/PhysRevB.93.245307

I. INTRODUCTION

The interest in two-dimensional materials presenting electronic properties different from the ones of graphene [1–3] has increased enormously in recent years. Indeed, although graphene possesses an extremely high electron mobility, it lacks a finite band gap, making its use in transistors difficult. Therefore, researchers have become interested in other two-dimensional materials, such as transition-metal dichalcogenides (TMDs) [4,5], hexagonal boron nitride (h-BN) [4], and phosphorene [6–9], among others [10,11]. Because of their reduced dimensionality, they display peculiar properties: for instance, the band gap of a single layer of MoS_2 is direct, while it is indirect in its bulk form [12]. At the same time, optical properties are also significantly different when going from the bulk to the single-layer limit: due to the lack of screening along one direction, exciton binding energies are usually much larger than in the bulk [13,14].

Although tremendous progress has already been achieved in synthesizing and studying two-dimensional compounds, expanding the landscape of known two-dimensional materials is needed in order to have access to a wider range of properties [15]. For instance, it was shown recently that metal phosphorus trichalcogenides (MPX_3) [16–18], In_2Se_3 [19,20], and TiS_3 [21,22] are very promising materials for some applications in optics and electronics.

In this paper, we study the properties of several trichalcogenide and sesquichalcogenide compounds. In particular, we will focus on the dynamical stability and electronic structure of $AlSiTe_3$, $InSiTe_3$, As_2S_3, As_2Se_3, β-As_2Te_3, β-Al_2Te_3, and B_2S_3. All of these compounds exist already in the form of bulk crystals (see Fig. 1) and their structures have been characterized using x-ray diffraction [23], but very little is known about the properties of the corresponding monolayers. Here we aim to achieve such an understanding using *ab initio* calculations. Our paper is organized as follows: in Sec. II, we describe the different computational methods that we have used in our work, while in Sec. III we present our results, followed by a conclusion in Sec. IV.

II. COMPUTATIONAL DETAILS

The present calculations are based on density functional theory (DFT) and the projector-augmented wave (PAW) method as implemented in the Vienna Ab Initio Simulation Package (VASP) [24]. The Perdew-Burke-Ernzerhof (PBE) [25] parametrization of the generalized gradient approximation (GGA) is used for the exchange-correlation potential with a plane-wave cutoff of 400 eV and a $12 \times 12 \times 1$ and $12 \times 7 \times 1$ k-point mesh for hexagonal and monoclinic structures. Similar parameters were used for the Heyd-Scuseria-Ernzerhof (HSE) calculations [26]. The two-dimensional slab geometries were set up with a vacuum space of more than 15 Å to ensure decoupling between periodically repeated systems. Then each system was fully relaxed with residual forces smaller than 0.0001 eV/Å. The dynamical stability of all single layers was determined using the PHONOPY code [27] with $5 \times 5 \times 1$ and $6 \times 2 \times 1$ supercells for the hexagonal and monoclinic structures, respectively, using density functional perturbation theory [28] (DFPT). Interlayer distance and binding energies were calculated with the revB86b-DF2 functional [29] found to give highly consistent values when benchmarked against the random-phase approximation [30] and using an in-house implementation [31] of the nonlocal correlation framework of Dion *et al.* [32]. The interlayer binding energy is then

$$E_B = \frac{E_{\text{monolayer}} - E_{\text{bulk}}/N}{A}, \tag{1}$$

where N is the number of layers in the bulk phase and A is the in-plane area of the monolayer unit cell.

III. RESULTS

The crystal structure and unit cell of the different monolayers investigated here are shown in Fig. 2 (for $AlSiTe_3$ and

*debbichi@kaist.ac.kr

†sebastien.lebegue@univ-lorraine.fr

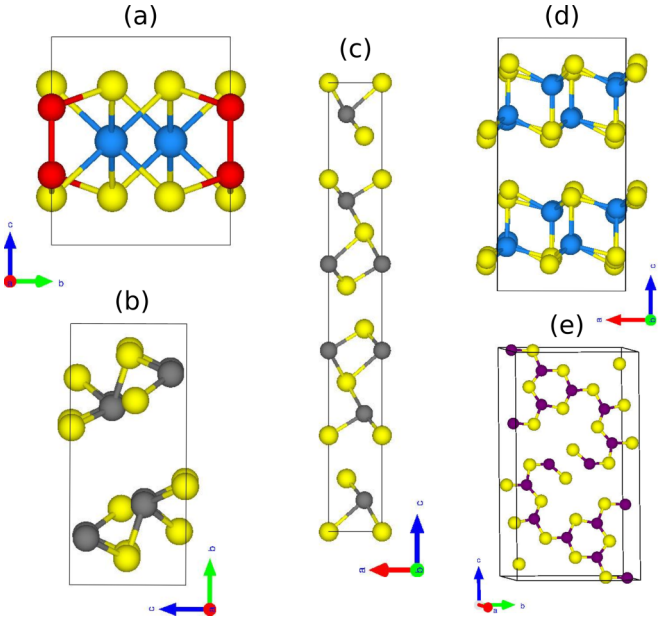

FIG. 1. Bulk crystal structure of (a) $AlSiTe_3$ (similar for $InSiTe_3$), (b) As_2S_3 (similar for As_2Se_3), (c) β-As_2Te_3, (d) β-Al_2Te_3, and (e) B_2S_3. The chalcogen atoms (S, Se, or Te), Si, Al (In), As, and B are represented by yellow, red, blue, gray, and purple spheres, respectively.

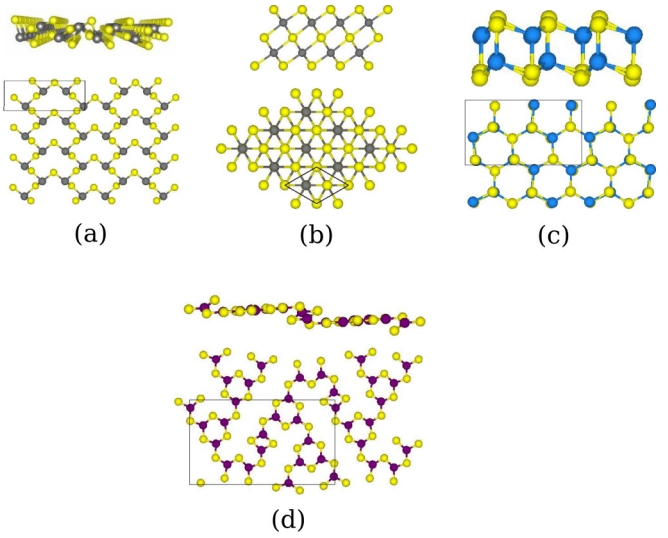

FIG. 3. Crystal structure of (a) orpiment As_2S_3 (similar for As_2Se_3), (b) β-As_2Te_3, (c) β-Al_2Te_3, and (d) B_2S_3 monolayers: top and side views. The chalcogen atoms (S, Se, or Te) are shown in yellow color, and As, Al, and B are shown in gray, blue, and purple color, respectively. Black lines indicate the primitive cell of the crystals.

$InSiTe_3$) and in Fig. 3 (for As_2S_3, As_2Se_3, β-As_2Te_3, β-Al_2Te_3, and B_2S_3).

The lattice of the $AlSiTe_3$ and $InSiTe_3$ monolayers is hexagonal, with each silicon atom bonded to one silicon and to three tellurium atoms, while the Al (or In) atoms are at the center of the octahedra formed by the tellurium atoms [see Fig. 2(a)]. Concerning As_2S_3 (and, equivalently, As_2Se_3), the structure presented in Fig. 3(a) corresponds to the orpiment phase, having a monoclinic structure with each As atom bonded to three sulfur atoms. The layer is highly corrugated,

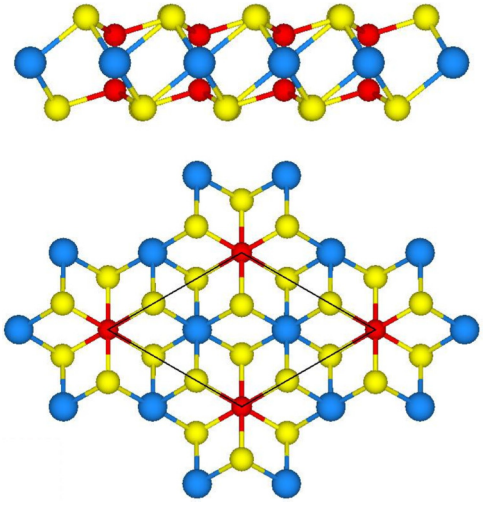

FIG. 2. Top and side view of a crystal structure of a monolayer of $AlSiTe_3$ (similar for $InSiTe_3$). The black lines indicate the primitive cell of the system. The chalcogen (Te), Si, and Al are represented by yellow, red, and blue spheres, respectively.

with sulfur atoms making bonds between As_2S_2 entities. The structure of β-As_2Te_3 differs drastically from its sulfur and selenium counterparts [Fig. 1(b)]: the layer is five atoms thick, with atoms ordered in the sequence Te-As-Te-As-Te in the direction perpendicular to the layer. The structure of β-Al_2Te_3 [see Fig. 3(c)] is monoclinic, although with a β angle of only 90.04°. The tellurium atoms are at the edge of the monolayer, while the aluminum atoms form the core of the material. Notice that the atoms are not positioned on perfectly flat planes and some slight puckering can be observed, which is related to the fact that the cell is not tetragonal but monoclinic. The crystal structure of B_2S_3 is pictured in Fig. 3(d). B_2S_3 has a monoclinic lattice ($\beta = 96.23°$) made of chains of S_3 triangles with a boron atom at the center, connected to each other by sulfur atoms. The monolayer is one atom thick, although the layer is not perfectly flat.

Our calculated binding energies per unit area and interlayer distances, defined as the nearest-neighbor gap between the layers, are presented in Table I. We found that the values fall within the range of values typical of van der Waals bonded solids [33] such as graphite, *h*-BN, and $MoSe_2$, which suggests these materials as strong candidates for compounds that can exist as freestanding layers [34]. To further strengthen this prediction, we have studied their dynamical stabilities. In Figs. 4 and 5, we present the calculated phonon-dispersion curves of all the compounds (in a monolayer form shown in Figs. 2 and 3) investigated here. No unstable phonon modes are observed in the phonon-dispersion curves, confirming the dynamical stability of the two-dimensional (2D) form of these materials (in a few cases, there appears to be a weakly unstable phonon branch in a small pocket very close to the Brillouin-zone center: this is not a real physical effect, but reflects the well-known difficulty in achieving numerical convergence for the flexural phonon mode for 2D materials [35]).

TABLE I. Interlayer binding energy E_b (in meV/Å^2) and interlayer distances d (defined as the nearest-neighbor distance across the gap (in Å) of the various systems investigated here as calculated with the revB86b-DF2 functional [29]. The binding energy and interlayer distances of some well-known layered materials are also shown for comparison.

Structure	E_b (meV/Å^2)	d (Å)
$AlSiTe_3$	17.6	4.01
$InSiTe_3$	18.3	4.01
As_2S_3	19.9	3.44
As_2Se_3	22.1	3.56
As_2Te_3	24.9	3.62
Al_2Te_3	15.2	4.00
B_2S_3	15.2	3.57
$MoSe_2$[a]	21.6	3.55
h-BN[a]	20.5	3.27
Graphite[a]	21.0	3.62

[a]Ref. [30].

In addition to the dynamical stability of these systems, we have also investigated their electronic properties. From our calculated PBE electronic band structures, we found that all of the monolayers are semiconductors. Considering the fact that the PBE functional usually underestimates the electronic band gap of semiconducting materials, the HSE06 functional was used to get more realistic values. The obtained band gaps are shown in Table II for both PBE and HSE06 functionals together with the nature [direct (D) or indirect (I)] of the gap. The HSE06 band structures are shown in Figs. 6 and 8. The energy gaps are found to be between 1.05 and 3.79 eV, in the range of visible light, with B_2S_3 having the largest (3.79 eV) and β-As_2Te_3 having the smallest (1.05 eV) band gap. Also, we have found that only B_2S_3 has a direct band gap at the Γ point of the Brillouin zone. Among this list of semiconductors, there are isostructural compounds such as $MSiTe_3$ (M = Al, In) and As_2X_3 (X = S, Se). In the case of

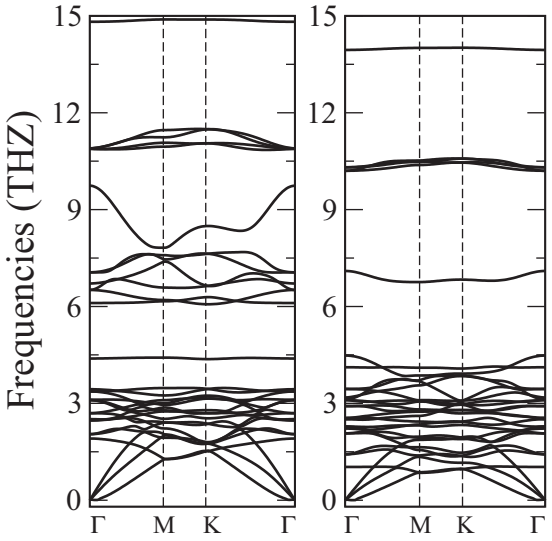

FIG. 4. Phonon-dispersion curves of $AlSiTe_3$ (left side) and $InSiTe_3$ (right side).

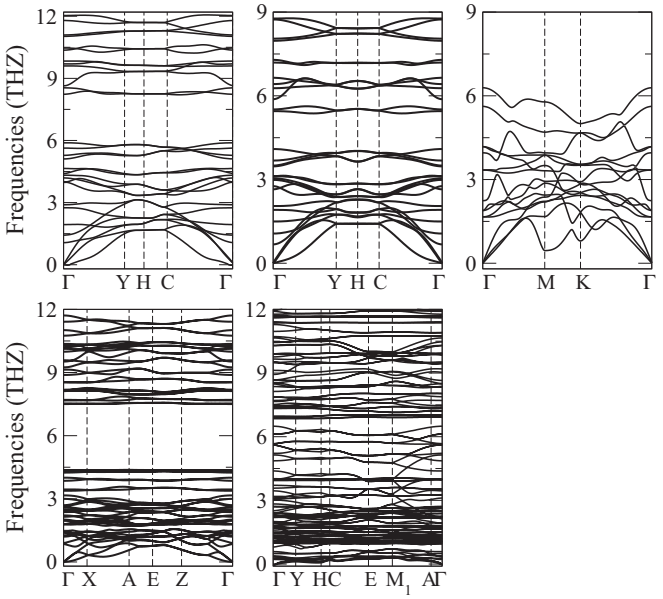

FIG. 5. Phonon-dispersion curves from the top to the left side of As_2S_3, As_2Se_3, β-As_2Te_3, β-Al_2Te_3, and B_2S_3 single layers.

$AlSiTe_3$ and $InSiTe_3$, we found that the band gap decreases from 2.05 to 1.54 eV when changing Al for In, followed by a change of the valence-band maximum (VBM) location, while the conduction-band minimum (CBM) is located in the same position (for $AlSiTe_3$, the VBM and CBM are found between M-Γ and K-M, respectively, while in $InSiTe_3$, the VBM and the CBM are found at the K and between K-M high-symmetry points). According to the calculated partial density of states (PDOS) shown in Fig. 7, the VBM comes from the chalcogen atoms while the CBM is a hybridization between the Al(In) and the Te atoms. However, in the case of As_2X_3 (X = S, Se), we have found that increasing the X atomic number only reduces the band gap by ∼0.7 eV. The PDOS of the A_2X_3 are shown in Fig. 9, and we found that for most of these compounds, the VBMs belong to the chalcogen atoms, while the CBMs belong to the M atoms: only in the case of Al_2Te_3 does the VBM and CBM belong to the M atoms.

Also, according to our calculated HSE06 band gap, some of these materials have a suitable band gap to be used in certain optoelectronics devices: among them, $InSiTe_3$, $AlSiTe_3$, β-Al_2Te_3, and As_2X_3 have a band gap in the

TABLE II. Crystal symmetries and calculated electronic band gap E_g (in eV) of the monolayers investigated here using the PBE and HSE functionals, and the nature of the gap [indirect (I) and direct (D) gap].

Structure	Symmetry	E_g^{PBE}	E_g^{HSE}	Band gap
$AlSiTe_3$	hex.	1.34	2.05	I
$InSiTe_3$	hex.	0.89	1.54	I
As_2S_3	mon.	2.12	2.95	I
As_2Se_3	mon.	1.64	2.25	I
β-As_2Te_3	rhom.	0.72	1.05	I
β-Al_2Te_3	mon.	1.91	2.61	I
B_2S_3	mon.	2.71	3.79	D

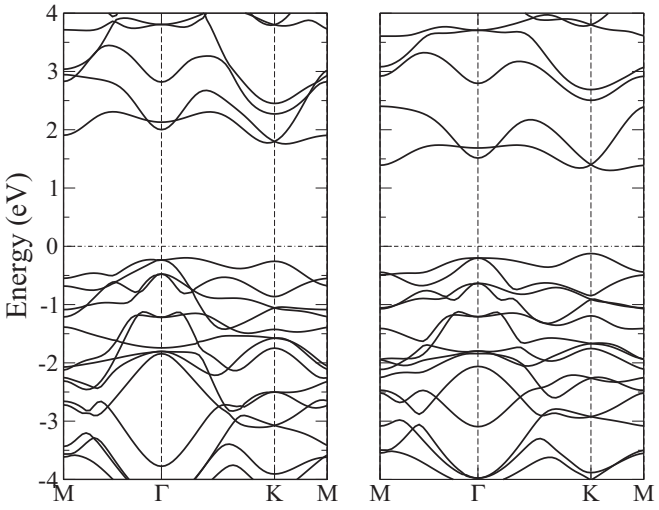

FIG. 6. Calculated electronic band structure of $AlSiTe_3$ (left) and $InSiTe_3$ (right) monolayers using the HSE06 functional. States with negative energies correspond to valence states, while states with a positive energy correspond to conduction states.

same range as transition-metal dichalcogenides [36–38] or phosphorene [8,39,40].

Furthermore, we have analyzed their electronic structures to investigate whether these compounds could be used for photocatalytic water-splitting applications. To be usable for water splitting, a semiconductor is required to have a sizable band gap exceeding the free energy of water splitting of 1.23 eV to allow the absorption of a large portion of the

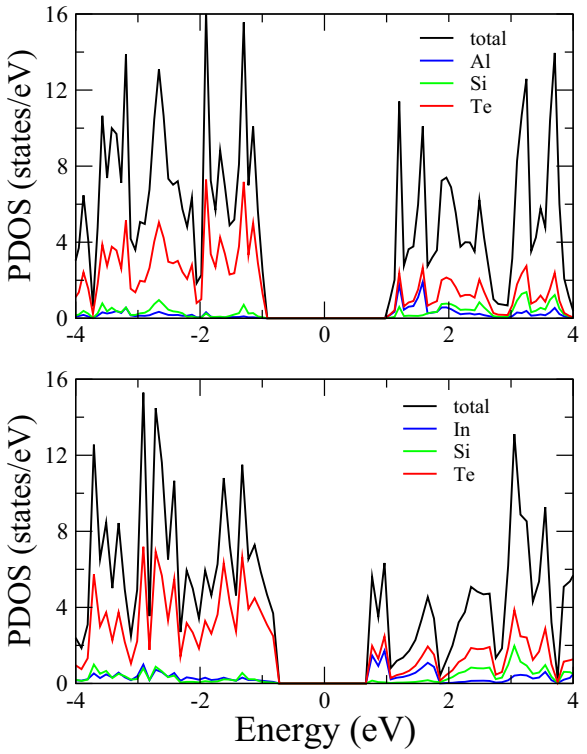

FIG. 7. Total and partial density of states of $AlSiTe_3$ (top) and $InSiTe_3$ (bottom) monolayers. The Fermi level is set at zero level.

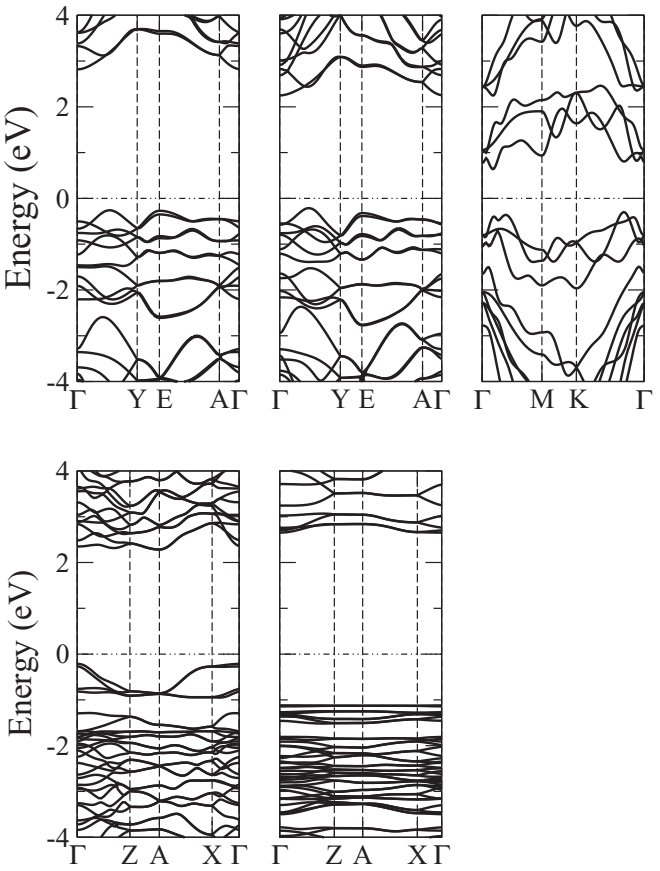

FIG. 8. Calculated electronic band structure of A_2X_3 monolayers using the HSE06 functional: from the top to the left, As_2S_3, As_2Se_3, β-As_2Te_3, β-Al_2Te_3, and B_2S_3. States with negative energies correspond to valence states, while states with a positive energy correspond to conduction states.

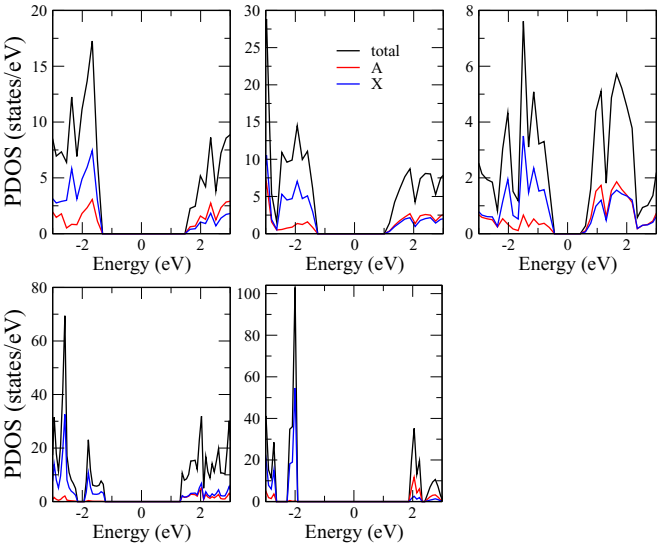

FIG. 9. Total and partial density of states (PDOS) of A_2X_3 monolayers: from the top to the left, As_2S_3, As_2Se_3, β-As_2Te_3, β-Al_2Te_3, and B_2S_3. The Fermi level is set at zero level.

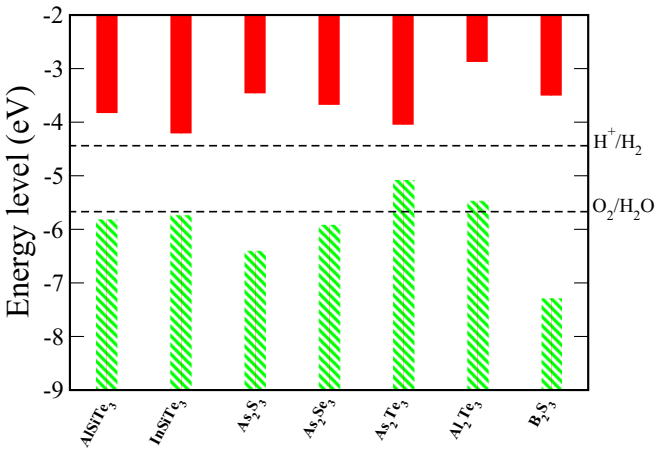

FIG. 10. Band edges of the semiconducting trichalcogenide single layers obtained with HSE06, with reference to the water redox potential. Valence- and conduction-band edges are shown with green and red color, respectively, and the dotted lines indicate the water reduction (H^+/H_2) and oxidation (H_2O/O_2) potentials at pH = 0.

solar spectrum [41]. In addition to the magnitude of the band gap, the band edges must straddle the redox potentials of water so that the reactions are thermodynamically accessible upon optical absorption [42,43]. To verify these properties, the CBM and VBM energy levels obtained by computing the work function [44] of each system using the HSE06 functional and compared to water's redox potential are shown in Fig. 10.

It is known that for a water-splitting reaction, the redox potential is dependent on the pH value [45–47]. The standard reduction and oxidation potential with respect to the vacuum level for H^+/H_2 and O_2/H_2O (at pH = 0) are calculated by using the following equation: $E^{red}_{H^+/H_2} = -4.44$ eV + pH $\times$ 0.059 and by $E^{ox}_{O_2/H_2O} = -5.67$ eV + pH $\times$ 0.059 eV, respectively.

As shown in Fig. 10, the comparison of the calculated valence-band edge (E_v) and conduction-band edge (E_c) with the redox potential of water at pH = 0 shows that $AlSiTe_3$, $InSiTe_3$, As_2S_3, As_2Se_3, and B_2S_3 layers have their band gap satisfying the requirement, and their band edges situated in energetically favorable positions for water splitting.

IV. CONCLUSION

In summary, we have used first-principles calculations to study a set of two-dimensional compounds. Their dynamical stability is demonstrated by the phonon-dispersion curves and the study of their electronic band structures shows that all of them are semiconductors with a band gap in the range of visible light. The interlayer binding energy is found to be typical of van der Waals bonding. Also, the calculation of their band edges show that several monolayers are good candidates for photocatalytic hydrogen generation.

ACKNOWLEDGMENTS

The authors acknowledge DARPA and Navy-NICOP for funding. O.E. gratefully acknowledges the Swedish Research Council (V.R.), SSF, and the Knut and Alice Wallenberg Foundation (Projects No. 2013.0020 and No. 2012.0031) for financial support. O.E. also acknowledges eSSENCE and STANDUPP. This work was performed using HPC resources from GENCI-CCRT/CINES (Grant No. x2016-085106). L.D. and H.K. acknowledge the support by the Global Frontier R&D Program (Grant No. 2013M3A6B1078884) on Center for Hybrid Interface Materials (HIM) funded by the Ministry of Science, ICT & Future Planning. T.B. gratefully acknowledges computational resources provided by Finland's IT Centre for Science (CSC).

[1] K. S. Novoselov, A. K. Geim, S. V. Morozov, D. Jiang, Y. Zhang, S. V. Dubonos, I. V. Grigorieva, and A. A. Firsov, Science **306**, 666 (2004).
[2] A. K. Geim and K. S. Novoselov, Nat. Mater. **6**, 183 (2007).
[3] G. W. Flynn, J. Chem. Phys. **135**, 050901 (2011).
[4] K. S. Novoselov, D. Jiang, F. Schedin, T. J. Booth, V. V. Khotkevich, S. V. Morozov, and A. K. Geim, Proc. Natl. Acad. Sci. USA **102**, 10451 (2005).
[5] J. N. Coleman, M. Lotya, A. ONeill, S. D. Bergin, P. J. King, U. Khan, K. Young, A. Gaucher, S. De, R. J. Smith, I. V. Shvets, S. K. Arora, G. Stanton, H.-Y. Kim, K. Lee, G. T. Kim, G. S. Duesberg, T. Hallam, J. J. Boland, J. J. Wang, J. F. Donegan, J. C. Grunlan, G. Moriarty, A. Shmeliov, R. J. Nicholls, J. M. Perkins, E. M. Grieveson, K. Theuwissen, D. W. McComb, P. D. Nellist, and V. Nicolosi, Science **331**, 568 (2011).
[6] F. Xia, H. Wang, and Y. Jia, Nat. Commun. **5**, 4458 (2014).
[7] L. Li, Y. Yu, G. J. Ye, Q. Ge, X. Ou, H. Wu, D. Feng, X. H. Chen, and Y. Zhang, Nat. Nanotechnol. **9**, 372 (2014).
[8] H. Liu, A. T. Neal, Z. Zhu, Z. Luo, X. Xu, D. Tománek, and P. D. Ye, ACS Nano **8**, 4033 (2014).
[9] S. P. Koenig, R. A. Doganov, H. Schmidt, A. H. C. Neto, and B. Özyilmaz, Appl. Phys. Lett. **104**, 103106 (2014).
[10] A. K. Geim and I. V. Grigorieva, Nature (London) **499**, 419 (2013).
[11] M. Xu, T. Liang, M. Shi, and H. Chen, Chem. Rev. **113**, 3766 (2013).
[12] S. Lebègue and O. Eriksson, Phys. Rev. B **79**, 115409 (2009).
[13] A. Ramasubramaniam, Phys. Rev. B **86**, 115409 (2012).
[14] M. M. Ugeda, A. J. Bradley, S.-F. Shi, F. H. da Jornada, Y. Zhang, D. Y. Qiu, W. Ruan, S.-K. Mo, Z. Hussain, Z.-X. Shen, F. Wang, S. G. Louie, and M. F. Crommie, Nat. Mater. **13**, 1091 (2014).
[15] S. Lebègue, T. Björkman, M. Klintenberg, R. M. Nieminen, and O. Eriksson, Phys. Rev. X **3**, 031002 (2013).
[16] J. Liu, X.-B. Li, D. Wang, W.-M. Lau, P. Peng, and L.-M. Liu, J. Chem. Phys. **140**, 054707 (2014).
[17] A. R. Wildes, V. Simonet, E. Ressouche, G. J. McIntyre, M. Avdeev, E. Suard, S. A. J. Kimber, D. Lançon, G. Pepe, B. Moubaraki, and T. J. Hicks, Phys. Rev. B **92**, 224408 (2015).
[18] Ke-zhao Du, Xing-zhi Wang, Y. Liu, P. Hu, M. I. B. Utama, C. K. Gan, Q. Xiong, and C. Kloc, ACS Nano **10**, 1738 (2016).
[19] L. Debbichi, O. Eriksson, and S. Lebègue, J. Phys. Chem. Lett. **6**, 3098 (2015).

[20] J. Zhou, Q. Zeng, D. Lv, L. Sun, L. Niu, W. Fu, F. Liu, Z. Shen, C. Jin, and Z. Liu, Nano Lett. **15**, 6400 (2015).
[21] E. Guilmeau, D. Berthebaud, P. R. N. Misse, S. Hébert, O. I. Lebedev, D. Chateigner, C. Martin, and A. Maignan, Chem. Mater. **26**, 5585 (2014).
[22] J. Dai and X. C. Zeng, Angew. Chem., Intl. Ed. **54**, 7572 (2015).
[23] F. H. Allen, Acta Crystallogr. Sect. B **58**, 380 (2002).
[24] G. Kresse and J. Hafner, Phys. Rev. B **47**, 558 (1993).
[25] J. P. Perdew, K. Burke, and M. Ernzerhof, Phys. Rev. Lett. **78**, 1396 (1997).
[26] J. Heyd, G. E. Scuseria, and M. Ernzerhof, J. Chem. Phys. **118**, 8207 (2003).
[27] A. Togo, F. Oba, and I. Tanaka, Phys. Rev. B **78**, 134106 (2008).
[28] X. Gonze and C. Lee, Phys. Rev. B **55**, 10355 (1997).
[29] I. Hamada, Phys. Rev. B **89**, 121103 (2014).
[30] T. Björkman, J. Chem. Phys. **141**, 074708 (2014).
[31] A. Gulans, M. J. Puska, and R. M. Nieminen, Phys. Rev. B **79**, 201105 (2009).
[32] M. Dion, H. Rydberg, E. Schröder, D. C. Langreth, and B. I. Lundqvist, Phys. Rev. Lett. **92**, 246401 (2004).
[33] T. Björkman, A. Gulans, A. V. Krasheninnikov, and R. M. Nieminen, Phys. Rev. Lett. **108**, 235502 (2012).
[34] B. C. Revard, W. W. Tipton, A. Yesypenko, and R. G. Hennig, Phys. Rev. B **93**, 054117 (2016).
[35] V. Zolyomi, N. D. Drummond, and V. I. Fal'ko, Phys. Rev. B **89**, 205416 (2014).
[36] Q. H. Wang, K. Kalantar-Zadeh, A. Kis, J. N. Coleman, and M. S. Strano, Nat. Nanotechnol. **7**, 699 (2012).
[37] D. Braga, I. G. Lezama, H. Berger, and A. F. Morpurgo, Nano Lett. **12**, 5218 (2012).
[38] J. Kang, S. Tongay, J. Zhou, J. Li, and J. Wu, Appl. Phys. Lett. **102**, 012111 (2013).
[39] V. Tran, R. Soklaski, Y. Liang, and L. Yang, Phys. Rev. B **89**, 235319 (2014).
[40] A. S. Rodin, A. Carvalho, and A. H. Castro Neto, Phys. Rev. Lett. **112**, 176801 (2014).
[41] A. K. Singh, K. Mathew, H. L. Zhuang, and R. G. Hennig, J. Phys. Chem. Lett. **6**, 1087 (2015).
[42] Y. Gai, J. Li, S.-S. Li, J.-B. Xia, and S.-H. Wei, Phys. Rev. Lett. **102**, 036402 (2009).
[43] R. M. Navarro Yerga, M. C. Álvarez Galván, F. del Valle, J. A. Villoria de la Mano, and J. L. G. Fierro, ChemSusChem **2**, 471 (2009).
[44] A. Walsh and C. R. A. Catlow, J. Mater. Chem. **20**, 10438 (2010).
[45] V. Chakrapani, J. C. Angus, A. B. Anderson, S. D. Wolter, B. R. Stoner, and G. U. Sumanasekera, Science **318**, 1424 (2007).
[46] J. Wang, N. Umezawa, and H. Hosono, Adv. Energy Mater. **6**, 1501190 (2016).
[47] X. Zhang, X. Zhao, D. Wu, Y. Jing, and Z. Zhou, Adv. Sci. (2016), doi:10.1002/advs.201600062.